Accommodating the CDF W-boson mass measurement in the beautiful mirror model

Shengdu Chai,[1,3,*] Jiayin Gu,[1,2,†] and Lian-Tao Wang[3,‡]

[1]Department of Physics and Center for Field Theory and Particle Physics, Fudan University, Shanghai 200438, China
[2]Key Laboratory of Nuclear Physics and Ion-beam Application (MOE), Fudan University, Shanghai 200433, China
[3]Department of Physics and Enrico Fermi Institute, University of Chicago, Chicago, Illinois 60637

(Received 22 February 2023; accepted 25 April 2023; published 9 May 2023)

The W-boson mass measurement recently reported by the CDF-II experiment exhibits a significant deviation from both the Standard Model prediction and previous measurements. There is also a long-standing deviation between the Standard Model prediction of the forward-backward asymmetry of the bottom quark ($A_{\mathrm{FB}}^{0,b}$) and its measurement at the LEP experiment. The beautiful mirror model, proposed to resolve the $A_{\mathrm{FB}}^{0,b}$ discrepancy, introduces vectorlike quarks that modify the W-boson mass at the one-loop level. In this study, we find an interesting region in the model parameter space that could potentially explain both discrepancies, which puts the new quarks in the multi-TeV region. This region is mostly consistent with current LHC bounds from direct searches and Higgs coupling measurements, but will be thoroughly probed at the high-luminosity LHC. As such, the beautiful mirror model as an explanation of the m_W and $A_{\mathrm{FB}}^{0,b}$ discrepancies could be confirmed or falsified in the near future.

DOI: 10.1103/PhysRevD.107.095013

I. INTRODUCTION

Recently, the CDF-II experiment reported a new measurement of the W-boson mass [1],

$$m_W^{\mathrm{CDF\text{-}II}} = 80433.5 \pm 9.4\ \mathrm{MeV}, \tag{1.1}$$

which exhibits a 7σ deviation from the Standard Model (SM) prediction, $m_W^{\mathrm{SM}} = 80357 \pm 6$ MeV, and a 4σ deviation from the PDG world average value [2], $m_W^{\mathrm{PDG}} = 80377 \pm 12$ MeV. The possible new physics explanations of this discrepancy have been extensively studied afterwards [3–126]. These explanations can be generally divided into two categories. One could introduce new physics that modifies the W mass at the tree level; this puts the new particle masses at or above the multi-TeV range which is beyond the reach of current or future LHC searches, but the new physics scenarios are limited to only a few possibilities, such as triplet scalar models (see e.g. Ref. [46]). A larger class of models could modify the W mass at the one-loop level, which leads to much richer phenomenological implications. In this case, larger couplings or smaller new-particle masses are usually required to generate a large enough modification to the W mass. This is generally in tension with direct search bounds, or other precision measurements if the new physics contributes at the tree level.

On the other hand, there is a long-standing 2.5σ discrepancy in the forward backward asymmetry of the bottom quark ($A_{\mathrm{FB}}^{0,b}$) between the SM prediction and the measured value at the LEP experiment [127]. Assuming this discrepancy is due to effects of beyond-the-Standard-Model (BSM) physics, it could be explained by introducing new exotic quarks that mix with the bottom quark, first proposed in Ref. [128] with the name "beautiful mirror" (BM). The new quarks contribute to the propagators of the electroweak (EW) gauge bosons and generate a nonzero T parameter, and thus modify the W-boson mass. This offers an intriguing possibility that the two measurement discrepancies could come from the same physics origin.

In this study, we further investigate the possibility that the BM Model gives rise to the measured discrepancies (from SM) for both $A_{\mathrm{FB}}^{0,b}$ at LEP and m_W at CDF-II. By performing a global fit of electroweak precision measurements, we find the preferred region of the parameter space. As shown later, it indeed provides a good fit to both measurements, significantly reducing the tension by only introducing a few model parameters in addition to the SM

*sdchai19@fudan.edu.cn
†jiayin_gu@fudan.edu.cn
‡liantaow@uchicago.edu

ones. We also study other phenomenological implications of this model, including the direct searches for exotic quarks and the precision Higgs measurements at the LHC. Roughly speaking, the parameter space preferred by the $A_{\rm FB}^{0,b}$ and CDF-II m_W measurements is consistent with current LHC measurements but can be thoroughly probed by future LHC runs, especially the HL-LHC. Therefore, the possibility that both the $A_{\rm FB}^{0,b}$ and CDF-II m_W discrepancies are explained by the BM model can be confirmed or falsified in the near future.

The rest of this paper is organized as follows: In Sec. II we review the BM model and work out its modifications to the relevant observables. In Sec. III, we perform an electroweak global fit to find the preferred region in the model parameter space. In Sec. IV, we summarize the current status of the relevant direct search bounds and Higgs coupling measurements as well as their future projections at the HL-LHC. The preferred regions of the model parameter space from various measurements are presented in Sec. V. Finally, we conclude in Sec. VI.

II. THE BEAUTIFUL MIRROR MODEL

The BM model was proposed in Ref [128] as a new-physics explanation of the $A_{\rm FB}^{0,b}$ measurement at LEP [127], which deviates significantly ($\sim 2.5\sigma$) from the SM prediction. New vectorlike exotic quarks are introduced, which mix with the bottom quark and modifies the $Zb\bar{b}$ couplings. Defining δg_{Lb} and δg_{Rb} as

$$\mathcal{L} = -\frac{g}{c_W} Z_\mu \left[\bar{b}_L \gamma^\mu \left(-\frac{1}{2} + \frac{1}{3} s_W^2 + \delta g_{Lb} \right) b_L + \bar{b}_R \gamma^\mu \left(\frac{1}{3} s_W^2 + \delta g_{Rb} \right) b_R \right] + \ldots, \tag{2.1}$$

where $s_W \equiv \sin\theta_W$, $c_W \equiv \cos\theta_W$ and θ_W is the weak mixing angle, positive values are preferred for both δg_{Lb} and δg_{Rb}, as shown later in Sec. III. This can be achieved by introducing two vectorlike quarks,

$$\Psi_{L,R} = \begin{pmatrix} B \\ X \end{pmatrix} \sim (3,2)_{-5/6}, \qquad \hat{B}_{L,R} \sim (3,1)_{-1/3}, \tag{2.2}$$

where the numbers in the bracket denote representations under $SU(3)_c$ and $SU(2)_W$, respectively, and the subscript denotes $U(1)_Y$ hypercharge. The mass and relevant interaction terms in the Lagrangian are given by

$$-\mathcal{L} \supset M_1 \bar{\Psi}_L \Psi_R + M_2 \bar{\hat{B}}_L \hat{B}_R + y_1 \bar{Q}_L H b_R + y_L \bar{Q}_L H \hat{B}_R + y_R \bar{\Psi}_L \tilde{H} b_R + \text{H.c.}. \tag{2.3}$$

After the electroweak symmetry breaking, the vacuum expectation value (VEV) of the Higgs field generates mixings between the new quarks and the SM bottom quark, and modifies the $Zb\bar{b}$ couplings as

$$\delta g_{Lb} = \frac{y_L^2 v^2}{4M_2^2}, \qquad \delta g_{Rb} = \frac{y_R^2 v^2}{4M_1^2}, \tag{2.4}$$

where $v = 246$ GeV. They can be obtained by either diagonalizing the mass matrix or using effective field theory (EFT) methods,[1] and are both positive as desired. Contributions to the gauge-boson propagators are generated at the one loop, which modifies the S and T parameters [130]. A direct computation gives

$$S \approx \frac{2}{9\pi} \left[-2\delta g_{Rb} \left(\log\left(\frac{y_1^2 v^2}{2M_1^2} \right) + 7 \right) + \delta g_{Lb} \left(4 \log\left(\frac{y_1^2 v^2}{2M_2^2} \right) + 2 \right) \right], \tag{2.5}$$

$$T \approx \frac{3}{16\pi^2 \alpha v^2} \left[\frac{16}{3} \delta g_{Rb}^2 M_1^2 + 4\delta g_{Lb}^2 M_2^2 - 4\delta g_{Lb} \frac{M_2^2 m_{\rm top}^2}{M_2^2 - m_{\rm top}^2} \log\left(\frac{M_2^2}{m_{\rm top}^2} \right) \right], \tag{2.6}$$

where we have omitted terms suppressed by the small bottom mass. Note that the S-parameter is generally small since we have only introduced vectorlike quarks. On the other hand, there is a sizable contribution to the T-parameter.

The BM model also modifies the Higgs couplings, and can therefore also be probed by precision Higgs measurements. At the tree level, only the $hb\bar{b}$ coupling is modified. A large set of Higgs couplings will be modified at the one-loop level. However, we expect the hgg and $h\gamma\gamma$ couplings to be the most relevant ones since they are relatively well-probed and their leading SM contributions are also at the one-loop level. For simplicity, we focus on the modifications of the $hb\bar{b}$, hgg and $h\gamma\gamma$ couplings, and compute them in the $m_h^2 \ll M_{1,2}$ limit. They can be parametrized by the familiar "kappa" parametrization,

$$\frac{\Gamma(h \to b\bar{b})}{\Gamma_{\rm SM}(h \to b\bar{b})} \equiv (1+\delta\kappa_b)^2, \quad \frac{\Gamma(h \to gg)}{\Gamma_{\rm SM}(h \to gg)} \equiv (1+\delta\kappa_g)^2, \quad \frac{\Gamma(h \to \gamma\gamma)}{\Gamma_{\rm SM}(h \to \gamma\gamma)} \equiv (1+\delta\kappa_\gamma)^2. \tag{2.7}$$

In particular, in the BM model they can be connected to δg_{Lb} and δg_{Rb} as (see also [131])

$$\delta\kappa_b \simeq -2(\delta g_{Lb} + \delta g_{Rb}), \qquad \delta\kappa_g \simeq 1.937(\delta g_{Lb} + \delta g_{Rb}), \qquad \delta\kappa_\gamma \simeq -0.137(\delta g_{Lb} + \delta g_{Rb}). \tag{2.8}$$

[1]The sum rules listed in Ref. [129] are also particularly convenient for the calculation in the EFT approach.

TABLE I. Best-fit values $\pm 1\sigma$ of and correlations among $S, T, \delta g_{Lb}, \delta g_{Rb}$ from EW global fit with the two different m_W scenarios.

		Correlation			
	1σ bound	S	T	δg_{Lb}	δg_{Rb}
		Old PDG			
S	-0.034 ± 0.084	1			
T	0.023 ± 0.068	0.926	1		
δg_{Lb}	0.0031 ± 0.0015	−0.345	−0.237	1	
δg_{Rb}	0.020 ± 0.0078	−0.394	−0.299	0.917	1
		New CDF			
S	0.070 ± 0.082	1			
T	0.198 ± 0.064	0.938	1		
δg_{Lb}	0.0037 ± 0.0015	−0.359	−0.271	1	
δg_{Rb}	0.021 ± 0.0078	−0.403	−0.326	0.918	1

III. ELECTROWEAK GLOBAL FIT

We perform a global fit to electroweak observables to determine the preferred region in the parameter space of the BM model. Following Ref. [132], the fit is done in the "SM + $S, T, \delta g_{Lb}, \delta g_{Rb}$" framework, where the SM is augmented by the four free parameters S, T, δg_{Lb}, and δg_{Rb}, which contain the leading contributions of the BM model. The results could then be easily translated into constraints on the model parameters. Our analysis mainly follows Refs. [22,133,134], and is a slightly simplified version of the ones in Refs. [131,132]. In particular, we have checked that our results are in good agreement with the one in Ref. [132]. We choose the $\{\alpha, m_Z, G_F\}$ input scheme and fix the values of the input parameters as [2]

$$\alpha = 1/127.940, \qquad m_Z = 91.1876 \text{ GeV},$$
$$G_F = 1.1663787 \times 10^{-5} \text{ GeV}. \tag{3.1}$$

We include the W and Z pole measurements, which are

$$\Gamma_Z, \quad \sigma_{\text{had}}, \quad R_f, \quad A_{FB}^{0,f}, \quad A_f, \quad A_{e/\tau}^{\text{pol}},$$
$$m_W, \quad \Gamma_W, \quad \text{Br}(W \to e\nu), \quad \text{Br}(W \to \mu\nu), \quad \text{Br}(W \to \tau\nu), \tag{3.2}$$

where $f = e, u, \tau, b, c$, and $A_{e/\tau}^{\text{pol}}$ is A_e and A_τ measured using final-state tau polarizations at LEP. For the Z-pole measurements, we use the results in Ref. [127]. For the W branching ratios measurements, we take the results from Ref. [135]. The measurement of Γ_W is taken from Ref. [2]. For the W boson mass m_W, we consider two different measurements, one is the "old" world average measurement from Ref. [2], the other is the "new CDF" measurement from Ref. [1]. Our results are shown in Table I in terms of the 1σ bounds of $S, T, \delta g_{Lb}, \delta g_{Rb}$, and their correlations. We further illustrate the results in Fig. 1 in terms of the 68% confidence level (CL) regions in the $S - T$ and $\delta g_{Lb} - \delta g_{Rb}$ planes. For comparison, the results in the SM + S, T framework (with δg_{Lb}, δg_{Rb} fixed to zero) and the ones in the SM + $T, \delta g_{Lb}, \delta g_{Rb}$ framework (with $S = 0$) are also shown. The latter scenario is closer to the case in

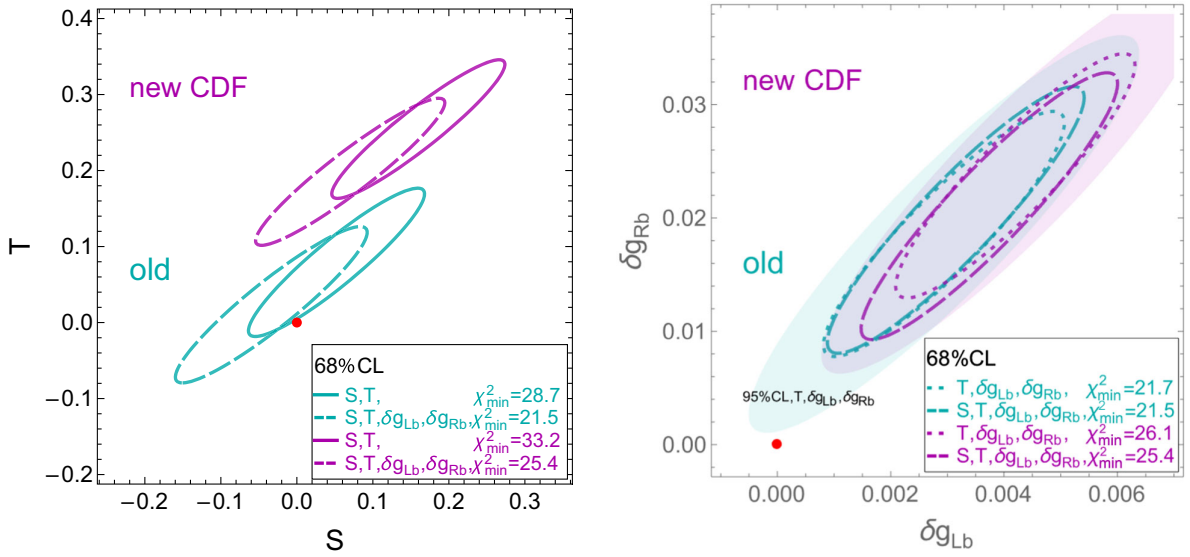

FIG. 1. Preferred regions in the $S - T$ and $\delta g_{Lb} - \delta g_{Rb}$ planes from a two-parameter fit with S and T (solid contours), a four-parameter fit with $S, T, \delta g_{Lb}, \delta g_{Rb}$ (dashed contours), and a three-parameter fit with $T, \delta g_{Lb}, \delta g_{Rb}$ (fixing $S = 0$, dotted contours) with the current EW measurements. Two different m_W scenarios are considered, which are the "new CDF" measurement and the "old PDG" m_W measurement before the CDF one. The red point is the SM prediction. All contours correspond to 68% CL, except for the shaded regions on the right panel which correspond to the 95% CL region of the three-parameter fit with $T, \delta g_{Lb}, \delta g_{Rb}$.

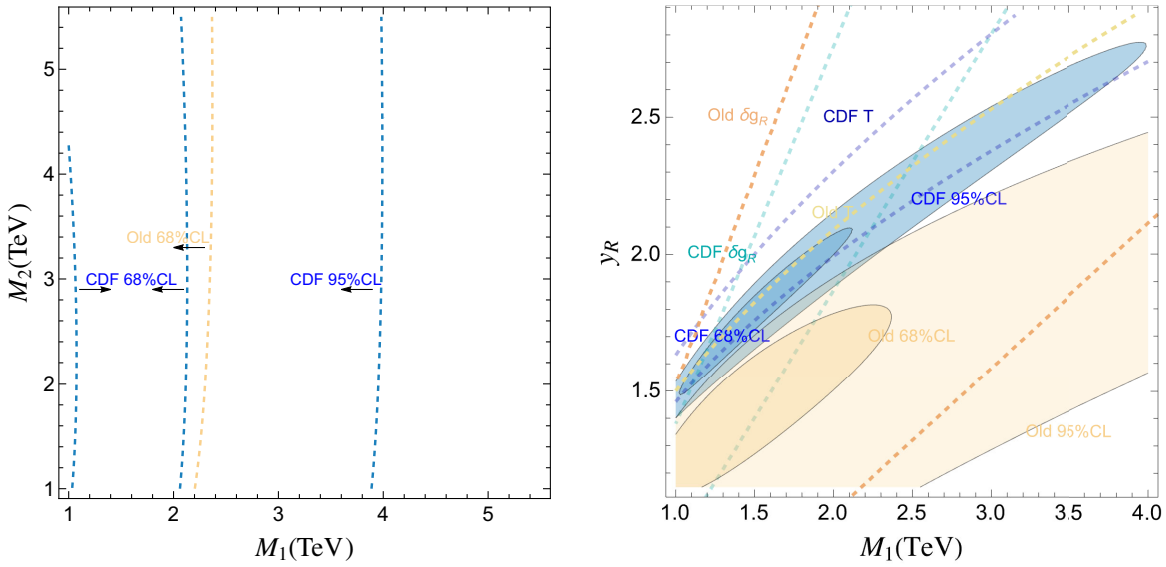

FIG. 2. *Left:* 68% and 95% CL preferred regions in the $M_1 - M_2$ plane from the EW fit with the new CDF m_W (blue) and the old PDG m_W (orange). The arrows point to the more preferred regions. For the "old" case, the 95% CL contour is at $M_1 \simeq 10$ TeV. *Right:* Preferred regions of parameter space in the $M_1 - y_R$ plane, with M_2 fixed at 4 TeV and y_L marginalized. The blue (orange) areas are the 68% and 95% CL regions from the EW global fit with the new CDF m_W (old PDG m_W), while the cyan, blue (orange, yellow) dashed lines correspond to 68% CL bounds from the δg_{Rb}, T-parameter constraint alone, respectively.

the BM model, which generally has a very small contribution to the S parameter, as mentioned above.

It is clear in Fig. 1 that, with only the S and T parameters, the new CDF W-mass measurement prefers a positive shift in both S and T. This is in agreement with many of the earlier EW-fit results, such as Refs. [3,7,9,16,22,24]. The inclusion of δg_{Lb}, δg_{Rb} brings down the overall $\chi^2_{\rm min}$ due to the better agreements in $A^{0,b}_{\rm FB}$, and also introduces a negative shift in S and T (as also observed in Ref. [132]). As a result, a zero S is within the 68% CL even with the new CDF m_W measurement. On the other hand, as shown in Fig. 1, the 68% CL preferred region in the $\delta g_{Lb} - \delta g_{Rb}$ plane changes only slightly under a shift in m_W, and the SM point (0,0) is clearly at the outside of it. However, the difference is notably larger for the $S = 0$ case, with the preferred regions of δg_{Lb} and δg_{Rb} both shifted to larger values with the new CDF m_W measurement. This has important implications in the BM model, as we will discuss below. In Fig. 2, we project the EW global-fit results (with the new CDF m_W) onto the parameter space of the BM model. The relevant parameters are the two Yukawa couplings y_R, y_L, and the two masses, M_1 and M_2. A crucial observation is that while δg_{Lb}, δg_{Rb}, and T all scales as $1/M^2_{1,2}$ at the leading order as they correspond to dimension-6 operators, their dependencies on the Yukawa couplings are different, with $\delta g_{Lb}, \delta g_{Rb} \sim y^2$ and $T \sim y^4$. This difference can be easily understood from the fact that δg_{Lb}, δg_{Rb} are generated at the tree level with two insertions of Yukawa couplings, while T is generated by a fermion loop with four insertions of Yukawa couplings (as $\mathcal{O}_T = \frac{1}{2}(H^\dagger \overleftrightarrow{D}_\mu H)^2$ contain four external Higgs legs). Therefore, the global fit could in principle separately constrain the Yukawa couplings and the mass terms. This is illustrated on the left panel of Fig. 2, where we marginalize over δg_{Lb} and δg_{Rb} and project the bounds from the "SM $+ S, T, \delta g_{Lb}, \delta g_{Rb}$" fit on the (M_1, M_2) plane. Results with the "new CDF" m_W (in blue) and the "old" PDG m_W (in orange) are shown in comparison. Note that, for fixed δg_{Lb} and δg_{Rb}, the bound is mostly provided by the T parameter. The result clearly shows that the EW measurements are mainly sensitive to M_1, which is expected from Eq. (2.6) since $\delta g_{Rb} \gg \delta g_{Lb}$, and the upper bound on the T parameter also puts an upper bound on m_W. On the other hand, it is peculiar that with the new CDF m_W, the upper bound on M_1 is stronger despite that it allows for a larger value of T. This is because, as shown in Fig. 1, the preferred value of δg_{Rb} is also larger with the new CDF m_W, especially for $S = 0$ which is approximately the case in the BM model. It is clear from Eq. (2.6) that for a fixed T this would decrease the value of M_1. In particular, for the "old" measurements, the 95% CL contour almost reaches the point $\delta g_{Lb} = \delta g_{Rb} = 0$, at which the T parameter would not provide an upper bound on M_1. Indeed, we observe a much larger 95% CL upper bound for M_1 with old measurements, which is at around 10 TeV. On the right panel of Fig. 2 we fix M_2 to a relatively large value, 4 TeV, and marginalize over y_L to find the preferred region in the (M_1, y_R) plane from the "SM $+ S, T, \delta g_{Lb}, \delta g_{Rb}$" fit. This is our main result, which has important implications. First, it is clear that y_R and M_1 can be separately constrained due to the interplay between δg_{Rb} and T. To illustrate this, we also show the 68% CL bounds from the δg_{Rb} alone and T alone,

which clearly constrain different combinations of y_R and M_1. As a result, with the new CDF m_W measurement (blue regions), the global fit puts an upper bound on M_1, with $M_1 \lesssim 4$ TeV within a 95% CL Crucially, this bound is consistent with the current LHC limits but could be relevant for future LHC probes, as we will discuss in the next section. On the other hand, with the old m_W, a larger M_1 is allowed, as mentioned above. The corresponding y_R is of order one in both cases, which ensures the perturbativity of the model.

IV. LHC PROBES

With the BM model being a potential explanation of both the $A_{\rm FB}^{0,b}$ and the m_W discrepancies, it is crucial to look for additional signals at the LHC that could confirm (or rule out) this possibility. The signals could come from either the direct searches of heavy exotic quarks or the precision Higgs measurements. They are discussed separately in this section.

A. Direct search bounds

In the BM model, QCD pair production has the largest rate in the small quark masses region, while single production of mirror quarks dominates for larger masses. In the multi-TeV region we are interested in, it turns out that the single production of the charge $-4/3$ quark X_R provides better reach, and we will focus on this channel. The relevant terms in the Lagrangian in the mass eigenstates are

$$-\frac{g s_R}{\sqrt{2}} \bar{X}_R \gamma^\mu W_\mu^- b_R + \text{H.c.}, \tag{4.1}$$

where $s_R = \frac{y_R v}{\sqrt{y_R^2 v^2 + 2M_1^2}}$ is the sine of the mixing angle between the right-handed quarks b_R and B_R. X decays dominantly to bW^- (or $\bar{b}W^+$), which is very similar to the decay of a charge $2/3$ top partner but with the opposite charge for the W. In the CMS study [136], the search on a charge $-4/3$ quark in the single production channel was done with a center-of-mass energy $\sqrt{s} = 13$ TeV and an integrated luminosity of 2.3 fb^{-1}. A lower-mass limit of 1.0 TeV is obtained assuming a coupling of 0.5 and 100% branching ratio to bW. The number of background events and the limits on signal $\sigma \times B(bW)$ are also provided in Ref. [136] up to $M_X = 1.8$ TeV, making it straightforward to extrapolate the bounds to the BM model parameter space and to the current integrated luminosity, at least up to around $M_1 \approx 1.8$ TeV. We use the VLQ model [137] in MadGraph 5 [138] to estimate the number of signal events for a benchmark point in the BM model. The resultant exclusion region is shown by the red shaded area in the left panel of Fig. 3, which assumes an integrated luminosity of 138 fb^{-1}. Furthermore, we extrapolate the bounds to the HL-LHC with an integrated luminosity of 3 ab^{-1}. This goes above the mass range covered in Ref. [136], and an accurate estimation of the background events is beyond the scope of this paper. Instead, we consider two scenarios with different assumptions on backgrounds. The first is simply

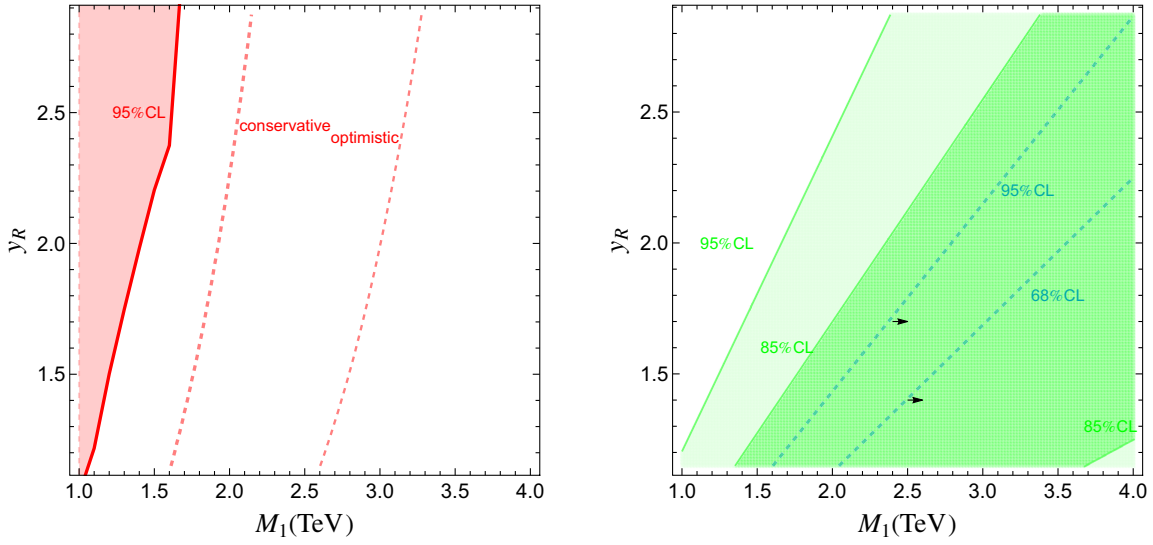

FIG. 3. *Left:* Direct search bounds from single productions of the charge $4/3$ quark in the $M_1 - y_R$ plane. The light red area is excluded at 95% CL by the CMS analysis [136] with an integrated luminosity of 138 fb^{-1}. The two dotted lines are the projected 95% CL reach at HL-LHC with different assumptions on the background. See text for more details. *Right:* Higgs coupling measurements bounds in the $M_1 - y_R$ plane with M_2 fixed at 4 TeV and y_L marginalized. The green (light green) areas are the region preferred by the current ATLAS Higgs couplings measurement [139] at 85% (95% CL). Note that, due to a small tension between the BM Model prediction ($\delta\kappa_g > 0$) the current Higgs measurement (which prefers $\delta\kappa_g < 0$), the lowest CL (with a $\Delta\chi^2$ measured from the $\chi^2_{\rm min}$ of the three-parameter Higgs coupling fit) is already at 83%. The area right to the cyan dotted lines represent the preferred region of future Higgs measurement at HL-LHC (assumed to be SM-like) with 68% and 95% CL as labeled.

TABLE II. Best-fit values $\pm 1\sigma$ of and correlations among κ_b, κ_g, κ_γ from the current ATLAS measurement [139] and the HL-LHC projections [141], assuming all other Higgs couplings are SM-like.

	Current (ATLAS)				HL-LHC			
		Correlation				Correlation		
	1σ bound	$\delta\kappa_b$	$\delta\kappa_g$	$\delta\kappa_\gamma$	1σ bound	$\delta\kappa_b$	$\delta\kappa_g$	$\delta\kappa_\gamma$
$\delta\kappa_b$	-0.14 ± 0.07	1			± 0.0165	1		
$\delta\kappa_g$	-0.069 ± 0.05	0.679	1		± 0.012	0.725	1	
$\delta\kappa_\gamma$	-0.014 ± 0.05	0.323	-0.128	1	± 0.0125	0.313	-0.064	1

no background, which gives the best possible reach; for the second, we assume a 400 GeV invariant-mass window is applied around m_X to efficiently remove backgrounds while keeping most signal events, and then simply extrapolate from the background in the range 1600 GeV to 2000 GeV in Ref. [136] to higher invariant masses, assuming the background cross section remains the same. This overestimates the background and will thus provide a conservative projection. Both results are shown with red dashed lines in the left panel of Fig. 3, with labels "optimistic" and "conservative", respectively.

B. Higgs coupling measurements

As mentioned in Sec. II, the BM model mainly contributes to κ_b, κ_g, and κ_γ in the Higgs measurements. Since these couplings contribute to multiple channels as well as the Higgs total width, we perform a three-parameter global fit to all the Higgs measurements to extract their bounds, assuming all other Higgs couplings are SM-like. For the current measurements, we use the ones collected in the ATLAS report [139]. Similar reaches are obtained by using the Higgs measurements at CMS [140]. For the HL-LHC Higgs measurements, we use the projections summarized in [141]. The results of the three-parameter fit are presented in Table II. Note that the HL-LHC Higgs measurements are assumed to be SM-like, so that the corresponding central values of $\delta\kappa_b$, $\delta\kappa_g$, $\delta\kappa_\gamma$ are zero by construction.

With Eq. (2.8) it is straightforward to map the Higgs coupling constraints in Table II to the BM model parameter space. In particular, we note that the BM model predicts negative $\delta\kappa_b$, $\delta\kappa_\gamma$, and a positive κ_g. Again, we fix $M_2 = 4$ TeV, marginalize y_L to project the bounds on the (M_1, y_R) plane, which are shown in the right panel of Fig. 3. The preferred region from the current measurements is shown with light green shades. Note that, the current ATLAS measurement prefers a negative $\delta\kappa_g$, which has some tension with the prediction of the BM model. As a result, the lowered CL in the (M_1, y_R) plane is already at 83% (with $\Delta\chi^2 = 3.55$ with respect to the $\chi^2_{\rm min}$ of the three-parameter Higgs coupling fit), while a region in the upper-left corner can be excluded by 95% CL (We have also shown the 85% CL contours.) On the other hand, assuming SM-like results, the HL-LHC prefers the bottom-right region with small y_R and large M_1, and the corresponding 68% and 95% CL bounds are shown with cyan dotted lines.

V. COMBINED RESULTS

We now combine the results of the EW precision measurements in Fig. 2 with the bounds from direct searches and Higgs measurements in Fig. 3. Our final result is presented in Fig. 4. The main message of our result is that the region in the BM model parameter space preferred by the $A_{\rm FB}^{0,b}$ and CDF-II m_W measurements is still consistent with the current direct search bounds and Higgs measurement constraints at the LHC. However, the model exhibits some small tension with the Higgs

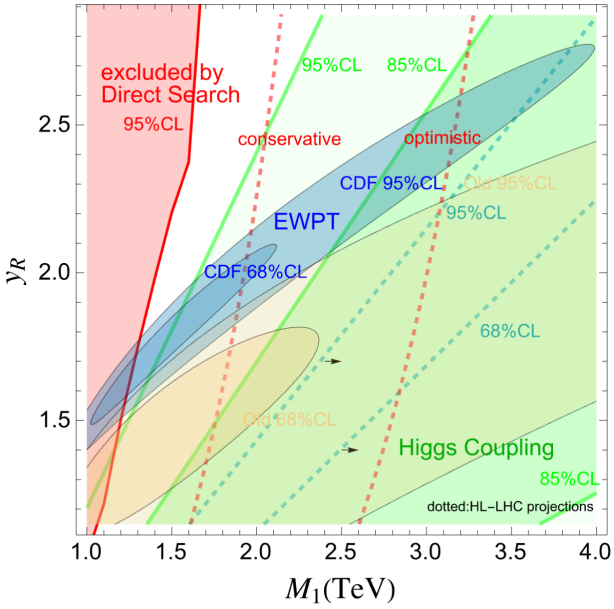

FIG. 4. Combined results in $M_1 - y_R$ plane from the current EW global fit with the new CDF/old PDG m_W measurement (preferred regions shown by the blue/orange area, from Fig. 2), current LHC direct search bounds (excluded region shown by the red area, from Fig. 3), and current LHC Higgs coupling measurements (preferred regions shown by the green areas, from Fig. 3). The red dotted lines are projected direct-search reaches of the HL-LHC. The area right to the cyan dotted lines are the preferred regions from the Higgs measurements at HL-LHC, assuming they are SM-like.

measurements, as it predicts an enhancement on the hgg coupling which is disfavored by current measurements. The direct search limit can be significantly improved at the HL-LHC, but even with the most optimistic assumption (with zero background), it will not be able to completely cover the relevant parameter space (95% CL preferred region of current EW measurements). The Higgs couplings measurements provide slightly better reaches. The region preferred by the HL-LHC Higgs couplings measurements, if SM-like, has little overlap with the one preferred by current EW measurements. Overall, the possibility that the BM model explains the $A_{\rm FB}^{0,b}$ and CDF-II m_W discrepancies will likely be either confirmed or ruled out by the HL-LHC. Crucially, this is not the case with the old m_W measurements, for which the (95% CL) allowed region by the EW measurements extends to much larger values of M_1. The CDF-II m_W result thus provides a strong motivation to search for the BM model at the HL-LHC.

VI. CONCLUSION

The m_W measurement at CDF-II and the $A_{\rm FB}^{0,b}$ measurement at LEP both exhibit significant discrepancies with the SM predictions. Needless to say, further investigations on the experimental side are needed for both measurements before one could make more definitive statements on the origins of the discrepancies. Meanwhile, the possibility that both discrepancies could come from the same underlying new physics is also interesting and worth exploring. In this paper, we consider the beautiful mirror model as a possible explanation to both discrepancies. By performing a global electroweak fit that includes the $A_{\rm FB}^{0,b}$ and the CDF-II m_W measurements, we find that this model indeed provides a much better fit to the measurements compared with SM. To achieve it, the mass of the exotic quark (with charge $-4/3$) is required to be below 4 TeV at the 95% confidence level, and the best-fit point corresponds to a mass of around 1.5 TeV. While the model is consistent with the current direct-search limits at the LHC, the future LHC runs, especially the HL-LHC, will be able to cover most of the regions of the parameter space preferred by the electroweak fit. The contributions to the Higgs couplings in this model are also relevant, especially for the hgg, $hb\bar{b}$, and $h\gamma\gamma$ couplings. Once again, the preferred region is consistent with the current LHC measurements but would be in tension with the projected precisions of the Higgs measurement at the HL-LHC, if they turn out to be SM-like. In summary, the possibility that both the $A_{\rm FB}^{0,b}$ and the CDF-II m_W discrepancies are explained by the beautiful mirror model will very likely be either confirmed or ruled out after the HL-LHC runs.

It should also be noted that, while both m_W and observables similar to $A_{\rm FB}^{0,b}$ could be measured at the LHC [142–146] or the Electron-Ion Collider (EIC) [147,148], these measurements are difficult and even with the future runs they may not reach the desired precision to resolve the discrepancies. Future lepton colliders, especially those with Z-pole and WW threshold runs (such as CEPC [149] and FCC-ee [150]), will be able to significantly improve the measurement precisions of these two observables, as well as the ones of other EW or Higgs measurements. Such a collider will be able to unambiguously resolve the current observed discrepancies in $A_{\rm FB}^{0,b}$ and m_W.

ACKNOWLEDGMENTS

We thank Henning Bahl for the useful discussions. J. G. is supported by the National Natural Science Foundation of China (NSFC) under Grant No. 12035008. L. T. W. is supported by the DOE Grant DE-SC0013642.

[1] T. Aaltonen *et al.* (CDF Collaboration), High-precision measurement of the W boson mass with the CDF II detector, Science **376**, 170 (2022).
[2] R. L. Workman *et al.* (Particle Data Group Collaboration), Review of particle physics, Prog. Theor. Exp. Phys. **2022**, 083C01 (2022).
[3] C.-T. Lu, L. Wu, Y. Wu, and B. Zhu, Electroweak precision fit and new physics in light of the W boson mass, Phys. Rev. D **106**, 035034 (2022).
[4] A. D'Alise *et al.*, Standard model anomalies: Lepton flavour non-universality, $g-2$ and W-mass, J. High Energy Phys. 08 (2022) 125.
[5] C.-R. Zhu, M.-Y. Cui, Z.-Q. Xia, Z.-H. Yu, X. Huang, Q. Yuan, and Y. Z. Fan, GeV Antiproton/Gamma-Ray Excesses and the W-Boson Mass Anomaly: Three Faces of ∼60–70 GeV Dark Matter Particle?, Phys. Rev. Lett. **129**, 231101 (2022).
[6] Y.-Z. Fan, T.-P. Tang, Y.-L. S. Tsai, and L. Wu, Inert Higgs Dark Matter for CDF II W-Boson Mass and Detection Prospects, Phys. Rev. Lett. **129**, 091802 (2022).
[7] A. Strumia, Interpreting electroweak precision data including the W-mass CDF anomaly, J. High Energy Phys. 08 (2022) 248.
[8] P. Athron, A. Fowlie, C.-T. Lu, L. Wu, Y. Wu, and B. Zhu, The W boson mass and muon $g-2$: Hadronic uncertainties or new physics?, Nat. Commun. **14**, 659 (2023).
[9] J. de Blas, M. Pierini, L. Reina, and L. Silvestrini, Impact of the Recent Measurements of the Top-Quark and

W-Boson Masses on Electroweak Precision Fits, Phys. Rev. Lett. **129**, 271801 (2022).
[10] T.-P. Tang, M. Abdughani, L. Feng, Y.-L. S. Tsai, J. Wu, and Y.-Z. Fan, NMSSM neutralino dark matter for W-boson mass and muon $g-2$ and the promising prospect of direct detection, Sci. China Phys. Mech. Astron. **66**, 239512 (2023).
[11] X. K. Du, Z. Li, F. Wang, and Y. K. Zhang, Explaining the muon $g-2$ anomaly and new CDF II W-boson mass in the framework of (extra)ordinary gauge mediation, Nucl. Phys. **B989**, 116151 (2023).
[12] C. Campagnari and M. Mulders, An upset to the standard model: Latest measurement of the W boson digs at the most important theory in particle physics, Science **376**, abm0101 (2022).
[13] G. Cacciapaglia and F. Sannino, The W boson mass weighs in on the non-standard Higgs, Phys. Lett. B **832**, 137232 (2022).
[14] M. Blennow, P. Coloma, E. Fernández-Martínez, and M. González-López, Right-handed neutrinos and the CDF II anomaly, Phys. Rev. D **106**, 073005 (2022).
[15] K. Sakurai, F. Takahashi, and W. Yin, Singlet extensions and W boson mass in light of the CDF II result, Phys. Lett. B **833** (2022) 137324,
[16] J. Fan, L. Li, T. Liu, and K.-F. Lyu, W-boson mass, electroweak precision tests and SMEFT, Phys. Rev. D **106**, 073010 (2022).
[17] B.-Y. Zhu, S. Li, J.-G. Cheng, R.-L. Li, and Y.-F. Liang, Using gamma-ray observation of dwarf spheroidal galaxy to test a dark matter model that can interpret the W-boson mass anomaly, arXiv:2204.04688.
[18] F. Arias-Aragón, E. Fernández-Martínez, M. González-López, and L. Merlo, Dynamical minimal flavour violating inverse seesaw, J. High Energy Phys. 09 (2022) 210.
[19] X. Liu, S.-Y. Guo, B. Zhu, and Y. Li, Correlating gravitational waves with W-boson Mass, FIMP dark matter, and Majorana Seesaw mechanism, Sci. Bull. **67**, 1437 (2022).
[20] A. Paul and M. Valli, Violation of custodial symmetry from W-boson mass measurements, Phys. Rev. D **106**, 013008 (2022).
[21] K. S. Babu, S. Jana, and V. P. K., Correlating W-Boson Mass Shift with Muon $g-2$ in the Two Higgs Doublet Model, Phys. Rev. Lett. **129**, 121803 (2022).
[22] J. Gu, Z. Liu, T. Ma, and J. Shu, Speculations on the W-mass measurement at CDF, Chin. Phys. C **46**, 123107 (2022).
[23] L. Di Luzio, R. Gröber, and P. Paradisi, Higgs physics confronts the M_W anomaly, Phys. Lett. B **832**, 137250 (2022).
[24] E. Bagnaschi, J. Ellis, M. Madigan, K. Mimasu, V. Sanz, and T. You, SMEFT analysis of m_W, J. High Energy Phys. 08 (2022) 308.
[25] J. J. Heckman, Extra W-boson mass from a D3-brane, Phys. Lett. B **833**, 137387 (2022).
[26] H. Bahl, J. Braathen, and G. Weiglein, New physics effects on the W-boson mass from a doublet extension of the SM Higgs sector, Phys. Lett. B **833**, 137295 (2022).
[27] H. Song, W. Su, and M. Zhang, Electroweak phase transition in 2HDM under Higgs, Z-pole, and W precision measurements, J. High Energy Phys. 10 (2022) 048.
[28] P. Asadi, C. Cesarotti, K. Fraser, S. Homiller, and A. Parikh, Oblique lessons from the W mass measurement at CDF II, arXiv:2204.05283.
[29] P. Athron, M. Bach, D. H. J. Jacob, W. Kotlarski, D. Stöckinger, and A. Voigt, Precise calculation of the W boson pole mass beyond the standard model with flexibleSUSY, Phys. Rev. D **106**, 095023 (2022).
[30] Y. Heo, D.-W. Jung, and J. S. Lee, Impact of the CDF W-mass anomaly on two Higgs doublet model, Phys. Lett. B **833**, 137274 (2022).
[31] A. Crivellin, M. Kirk, T. Kitahara, and F. Mescia, Large $t \to cZ$ as a sign of vectorlike quarks in light of the W mass, Phys. Rev. D **106**, L031704 (2022).
[32] M. Endo and S. Mishima, New physics interpretation of W-boson mass anomaly, Phys. Rev. D **106**, 115005 (2022).
[33] X. K. Du, Z. Li, F. Wang, and Y. K. Zhang, Explaining the new CDF II W-boson mass data in the Georgi-Machacek extension models, Eur. Phys. J. C **83**, 139 (2023).
[34] K. Cheung, W.-Y. Keung, and P.-Y. Tseng, Isodoublet vector leptoquark solution to the muon $g-2$, $R_{K,K*}$, $R_{D,D*}$, and W-mass anomalies, Phys. Rev. D **106**, 015029 (2022).
[35] L. Di Luzio, M. Nardecchia, and C. Toni, Light vectors coupled to anomalous currents with harmless Wess-Zumino terms, Phys. Rev. D **105**, 115042 (2022).
[36] R. Balkin, E. Madge, T. Menzo, G. Perez, Y. Soreq, and J. Zupan, On the implications of positive W mass shift, J. High Energy Phys. 05 (2022) 133.
[37] T. Biekötter, S. Heinemeyer, and G. Weiglein, Excesses in the low-mass Higgs-boson search and the W-boson mass measurement, arXiv:2204.05975.
[38] N. V. Krasnikov, Nonlocal generalization of the SM as an explanation of recent CDF result, arXiv:2204.06327.
[39] M.-D. Zheng, F.-Z. Chen, and H.-H. Zhang, The $W\ell\nu$-vertex corrections to W-boson mass in the R-parity violating MSSM, arXiv:2204.06541.
[40] Y. H. Ahn, S. K. Kang, and R. Ramos, Implications of the new CDF II W-boson mass on two-Higgs-doublet models, Phys. Rev. D **106**, 055038 (2022).
[41] X.-F. Han, F. Wang, L. Wang, J. M. Yang, and Y. Zhang, Joint explanation of W-mass and muon $g-2$ in the 2HDM*, Chin. Phys. C **46**, 103105 (2022).
[42] J. Kawamura, S. Okawa, and Y. Omura, W boson mass and muon $g-2$ in a lepton portal dark matter model, Phys. Rev. D **106**, 015005 (2022).
[43] A. Ghoshal, N. Okada, S. Okada, D. Raut, Q. Shafi, and A. Thapa, Type III seesaw with R-parity violation in light of m_W (CDF), Nucl. Phys. **B989**, 116099 (2023).
[44] P. Fileviez Perez, H. H. Patel, and A. D. Plascencia, On the W mass and new Higgs bosons, Phys. Lett. B **833**, 137371 (2022).
[45] K. I. Nagao, T. Nomura, and H. Okada, A model explaining the new CDF II W boson mass linking to muon $g-2$ and dark matter, arXiv:2204.07411.
[46] S. Kanemura and K. Yagyu, Implication of the W boson mass anomaly at CDF II in the Higgs triplet

model with a mass difference, Phys. Lett. B **831**, 137217 (2022).
[47] P. Mondal, Enhancement of the W boson mass in the Georgi-Machacek model, Phys. Lett. B **833**, 137357 (2022).
[48] R. A. Wilson, A toy model for the W/Z mass ratio, arXiv:2204.07970.
[49] K.-Y. Zhang and W.-Z. Feng, Explaining W boson mass anomaly and dark matter with a $U(1)$ dark sector, Chin. Phys. C **47**, 023107 (2023).
[50] V. Cirigliano, W. Dekens, J. de Vries, E. Mereghetti, and T. Tong, Beta-decay implications for the W-boson mass anomaly, Phys. Rev. D **106**, 075001 (2022).
[51] D. Borah, S. Mahapatra, D. Nanda, and N. Sahu, Type II Dirac seesaw with observable ΔNeff in the light of W-mass anomaly, Phys. Lett. B **833**, 137297 (2022).
[52] T. A. Chowdhury, J. Heeck, A. Thapa, and S. Saad, W boson mass shift and muon magnetic moment in the Zee model, Phys. Rev. D **106**, 035004 (2022).
[53] G. Arcadi and A. Djouadi, The $2HD + a$ model for a combined explanation of the possible excesses in the CDF $\mathbf{M_W}$ measurement and $(\mathbf{g-2})_\mu$ with dark matter, Phys. Rev. D **106**, 095008 (2022).
[54] O. Popov and R. Srivastava, The Triplet Dirac Seesaw in the view of the recent CDF-II W mass anomaly, Phys. Lett. B **840**, 137837 (2023).
[55] L. M. Carpenter, T. Murphy, and M. J. Smylie, Changing patterns in electroweak precision fits with new color-charged states: Oblique corrections and the W-boson mass, Phys. Rev. D **106**, 055005 (2022).
[56] A. Bhaskar, A. A. Madathil, T. Mandal, and S. Mitra, Combined explanation of W-mass, muon $g-2$, $R_{K^{(*)}}$ and $R_{D^{(*)}}$ anomalies in a singlet-triplet scalar leptoquark model, Phys. Rev. D **106**, 115009 (2022).
[57] K. Ghorbani and P. Ghorbani, W-boson mass anomaly from scale invariant 2HDM, Nucl. Phys. **B984**, 115980 (2022).
[58] M. Du, Z. Liu, and P. Nath, CDF W mass anomaly with a Stueckelberg-Higgs portal, Phys. Lett. B **834**, 137454 (2022).
[59] Y.-P. Zeng, C. Cai, Y.-H. Su, and H.-H. Zhang, Extra boson mix with Z boson explaining the mass of W boson, Phys. Rev. D **107**, 056004 (2023).
[60] A. Batra, S. K. A., S. Mandal, and R. Srivastava, W boson mass in Singlet-Triplet Scotogenic dark matter model, arXiv:2204.09376.
[61] D. Borah, S. Mahapatra, and N. Sahu, Singlet-doublet fermion origin of dark matter, neutrino mass and W-mass anomaly, Phys. Lett. B **831**, 137196 (2022).
[62] J. Cao, L. Meng, L. Shang, S. Wang, and B. Yang, Interpreting the W-mass anomaly in vectorlike quark models, Phys. Rev. D **106**, 055042 (2022).
[63] S. Baek, Implications of CDF W-mass and $(g-2)_\mu$ on $U(1)_{L_\mu - L_\tau}$ model, arXiv:2204.09585.
[64] J. Heeck, W-boson mass in the triplet seesaw model, Phys. Rev. D **106**, 015004 (2022).
[65] A. Addazi, A. Marciano, A. P. Morais, R. Pasechnik, and H. Yang, CDF II W-mass anomaly faces first-order electroweak phase transition, Eur. Phys. J. C **83**, 207 (2023).
[66] Y. Cheng, X.-G. He, F. Huang, J. Sun, and Z.-P. Xing, Dark photon kinetic mixing effects for the CDF W-mass measurement, Phys. Rev. D **106**, 055011 (2022).
[67] E. d. S. Almeida, A. Alves, O. J. P. Eboli, and M. C. Gonzalez-Garcia, Impact of CDF-II measurement of M_W on the electroweak legacy of the LHC Run II, arXiv:2204.10130.
[68] S. Lee, K. Cheung, J. Kim, C.-T. Lu, and J. Song, Status of the two-Higgs-doublet model in light of the CDF mW measurement, Phys. Rev. D **106**, 075013 (2022).
[69] C. Cai, D. Qiu, Y.-L. Tang, Z.-H. Yu, and H.-H. Zhang, Corrections to electroweak precision observables from mixings of an exotic vector boson in light of the CDF W-mass anomaly, Phys. Rev. D **106**, 095003 (2022).
[70] R. Benbrik, M. Boukidi, and B. Manaut, W-mass and 96 GeV excess in type-III 2HDM, arXiv:2204.11755.
[71] T. Yang, S. Qian, S. Deng, J. Xiao, L. Gao, A. M. Levin, Q. Li, M. Lu, and Z. You, The physics case for a neutrino lepton collider in light of the CDF W mass measurement, Int. J. Mod. Phys. A **37**, 2245001 (2022).
[72] A. Batra, S. K. A, S. Mandal, H. Prajapati, and R. Srivastava, CDF-II W boson mass anomaly in the canonical scotogenic neutrino-dark matter model, arXiv:2204.11945.
[73] H. B. T. Tan and A. Derevianko, Implications of W-boson mass anomaly for atomic parity violation, Atoms **10**, 149 (2022).
[74] H. Abouabid, A. Arhrib, R. Benbrik, M. Krab, and M. Ouchemhou, Is the new CDF M_W measurement consistent with the two higgs doublet model?, Nucl. Phys. **B989**, 116143 (2023).
[75] T.-K. Chen, C.-W. Chiang, and K. Yagyu, Explanation of the W mass shift at CDF II in the extended Georgi-Machacek model, Phys. Rev. D **106**, 055035 (2022).
[76] R. S. Gupta, Running away from the T-parameter solution to the W mass anomaly, arXiv:2204.13690.
[77] V. Basiouris and G. K. Leontaris, Sterile neutrinos, $0\nu\beta\beta$ decay and the W-boson mass anomaly in a Flipped $SU(5)$ from F-theory, Eur. Phys. J. C **82**, 1041 (2022).
[78] J.-W. Wang, X.-J. Bi, P.-F. Yin, and Z.-H. Yu, Electroweak dark matter model accounting for the CDF W-mass anomaly, Phys. Rev. D **106**, 055001 (2022).
[79] F. J. Botella, F. Cornet-Gomez, C. Miró, and M. Nebot, Muon and electron $g-2$ anomalies in a flavor conserving 2HDM with an oblique view on the CDF M_W value, Eur. Phys. J. C **82**, 915 (2022).
[80] J. Kim, Compatibility of muon $g-2$, W mass anomaly in type-X 2HDM, Phys. Lett. B **832**, 137220 (2022).
[81] J. Kim, S. Lee, P. Sanyal, and J. Song, CDF W-boson mass and muon $g-2$ in a type-X two-Higgs-doublet model with a Higgs-phobic light pseudoscalar, Phys. Rev. D **106**, 035002 (2022).
[82] B. Barman, A. Das, and S. Sengupta, New W-Boson mass in the light of doubly warped braneworld model, arXiv:2205.01699.
[83] S.-P. He, A leptoquark and vector-like quark extended model for the simultaneous explanation of the W boson mass and muon $g-2$ anomalies, Chin. Phys. C **47**, 043102 (2023).
[84] X.-Q. Li, Z.-J. Xie, Y.-D. Yang, and X.-B. Yuan, Correlating the CDF W-boson mass shift with the

$b \to s\ell^+\ell^-$ anomalies, Phys. Lett. B **838**, 137651 (2023).
[85] R. Dcruz and A. Thapa, W boson mass shift, dark matter and $(g-2)_\ell$ in ScotoZee model, Phys. Rev. D **107**, 015002 (2023).
[86] A. W. Thomas and X. G. Wang, Constraints on the dark photon from parity violation and the W mass, Phys. Rev. D **106**, 056017 (2022).
[87] J. Isaacson, Y. Fu, and C. P. Yuan, ResBos2 and the CDF W Mass Measurement, arXiv:2205.02788.
[88] T. Appelquist, J. Ingoldby, and M. Piai, Composite two-Higgs doublet model from dilaton effective field theory, Nucl. Phys. **B983**, 115930 (2022).
[89] J. Gao, D. Liu, and K. Xie, Understanding PDF uncertainty on the W boson mass measurements in CT18 global analysis, Chin. Phys. C **46**, 123110 (2022).
[90] J. L. Evans, T. T. Yanagida, and N. Yokozaki, W boson mass anomaly and grand unification, Phys. Lett. B **833**, 137306 (2022).
[91] S.-S. Kim, H. M. Lee, A. G. Menkara, and K. Yamashita, SU(2)D lepton portals for the muon $g-2$, W-boson mass, and dark matter, Phys. Rev. D **106**, 015008 (2022).
[92] T. A. Chowdhury and S. Saad, Leptoquark-vectorlike quark model for the CDF mW, $(g-2)\mu$, RK(*) anomalies, and neutrino masses, Phys. Rev. D **106**, 055017 (2022).
[93] G. Senjanović and M. Zantedeschi, $SU(5)$ grand unification and W-boson mass, Phys. Lett. B **837**, 137653 (2023).
[94] G. Lazarides, R. Maji, R. Roshan, and Q. Shafi, Heavier W boson, dark matter, and gravitational waves from strings in an SO(10) axion model, Phys. Rev. D **106**, 055009 (2022).
[95] R. Ghosh, B. Mukhopadhyaya, and U. Sarkar, The ρ parameter and the CDF W-mass anomaly: Observations on the role of scalar triplets, arXiv:2205.05041.
[96] V. Miralles, O. Eberhardt, H. Gisbert, A. Pich, and J. Ruiz-Vidal, Global fit on coloured scalars including the last W-boson mass measurement, in 56th Rencontres de Moriond on Electroweak Interactions and Unified Theories (2022), 5, arXiv:2205.05610.
[97] Y. Liu, Y. Wang, C. Zhang, L. Zhang, and J. Gu, Probing top-quark operators with precision electroweak measurements, Chin. Phys. C **46**, 113105 (2022).
[98] K. Asai, C. Miyao, S. Okawa, and K. Tsumura, Scalar dark matter with a $\mu\tau$ flavored mediator, Phys. Rev. D **106**, 035017 (2022).
[99] E. Ma, Type III neutrino Seesaw, freeze-in long-lived dark matter, and the W mass shift, Phys. Lett. B **833**, 137327 (2022).
[100] J. Kawamura and S. Raby, W mass in a model with vectorlike leptons and U(1)', Phys. Rev. D **106**, 035009 (2022).
[101] X. Chen, T. Gehrmann, N. Glover, A. Huss, T.-Z. Yang, and H. X. Zhu, Transverse mass distribution and charge asymmetry in W boson production to third order in QCD, Phys. Lett. B **840**, 137876 (2023).
[102] B. Allanach and J. Davighi, M_W helps select Z' models for $b \to s\ell\ell$ anomalies, Eur. Phys. J. C **82**, 745 (2022).
[103] S. S. Afonin, W-boson mass anomaly as a manifestation of spontaneously broken extended gauge symmetry on a new fundamental scale, Universe **8**, 627 (2022).
[104] H. M. Hill, W-boson mass hints at physics beyond the standard model, Phys. Today **75**, 14 (2022).
[105] S.-S. Xue, W boson mass tension caused by its right-handed gauge coupling at high energies?, Nucl. Phys. **B985**, 115992 (2022).
[106] T. G. Rizzo, Kinetic mixing, dark Higgs triplets, and MW, Phys. Rev. D **106**, 035024 (2022).
[107] D. Van Loi and P. Van Dong, Novel effects of the W-boson mass shift in the 3-3-1 model, Eur. Phys. J. C **83**, 56 (2023).
[108] S. Yaser Ayazi and M. Hosseini, W boson mass anomaly and vacuum structure in vector dark matter model with a singlet scalar mediator, arXiv:2206.11041.
[109] N. Chakrabarty, The muon $g-2$ and W-mass anomalies explained and the electroweak vacuum stabilised by extending the minimal Type-II seesaw, arXiv:2206.11771.
[110] S. Centelles Chuliá, R. Srivastava, and S. Yadav, CDF-II W boson mass in the Dirac Scotogenic model, arXiv:2206.11903.
[111] K. I. Nagao, T. Nomura, and H. Okada, An alternative gauged $U(1)_R$ symmetric model in light of the CDF II W boson mass anomaly, Phys. Rev. D **106**, 115011 (2022).
[112] M. T. Frandsen and M. Rosenlyst, Electroweak precision tests of composite Higgs models, J. High Energy Phys. 03 (2023) 222.
[113] H. Bahl, W. H. Chiu, C. Gao, L.-T. Wang, and Y.-M. Zhong, Tripling down on the W boson mass, Eur. Phys. J. C **82**, 944 (2022).
[114] S. Arora, M. Kashav, S. Verma, and B. C. Chauhan, Muon $(g-2)$ and W-boson mass anomaly in a model based on Z_4 symmetry with vector like fermion, Prog. Theor. Exp. Phys. **2022**, 113B06 (2022).
[115] W. Abdallah, R. Gandhi, and S. Roy, LSND and MiniBooNE as guideposts to understanding the muon $g-2$ results and the CDF II W mass measurement, Phys. Lett. B **840**, 137841 (2023).
[116] A. Batra, P. Bharadwaj, S. Mandal, R. Srivastava, and J. W. F. Valle, W-mass anomaly in the simplest linear seesaw mechanism, Phys. Lett. B **834**, 137408 (2022).
[117] K. Benakli, M. Goodsell, W. Ke, and P. Slavich, W boson mass in minimal Dirac gaugino scenarios, Eur. Phys. J. C **83**, 43 (2023).
[118] V. Barger, C. Hauptmann, P. Huang, and W.-Y. Keung, E_6 models in light of precision M_W measurements, Phys. Rev. D **107**, 075005 (2023).
[119] F. Domingo, U. Ellwanger, and C. Hugonie, M_W, dark matter and a_μ in the NMSSM, Eur. Phys. J. C **82**, 1074 (2022).
[120] M. C. Rodriguez, Explain the W-boson mass anomaly in the context of Supersymmetric $U(1)_{Y'} \otimes U(1)_{B-L}$ with three identical neutrinos, arXiv:2209.04653.
[121] G.-L. Liu, Constraints from new CDF II W-boson mass on top-bottom Seesaw and the TopFlavor Models, Int. J. Mod. Phys. A **37**, 2245002 (2022).
[122] H. Diaz, V. Pleitez, and O. P. Ravinez, On the W mass anomaly in models with right-handed currents, arXiv:2209.12121.
[123] W. Lin, T. T. Yanagida, and N. Yokozaki, The anomalous shift of the weak boson mass and the quintessence

electroweak axion, Commun. Theor. Phys. **75**, 035203 (2023).
[124] Y. Chung, Explaining the $R_{K^{(*)}}$ anomalies and the CDF M_W in flavorful top Seesaw models with gauged $U(1)_{L(-R)}$, arXiv:2210.13402.
[125] J. Butterworth, J. Heeck, S. H. Jeon, O. Mattelaer, and R. Ruiz, Testing the scalar triplet solution to CDF's fat W problem at the LHC, Phys. Rev. D **107**, 075020 (2023).
[126] T. Bandyopadhyay, A. Budhraja, S. Mukherjee, and T. S. Roy, A twisted tale of the transverse-mass tail, arXiv:2212.02534.
[127] S. Schael *et al.* (ALEPH, DELPHI, L3, OPAL, SLD, LEP Electroweak Working Group, SLD Electroweak Group, SLD Heavy Flavour Group Collaborations), Precision electroweak measurements on the Z resonance, Phys. Rep. **427**, 257 (2006).
[128] D. Choudhury, T. M. P. Tait, and C. E. M. Wagner, Beautiful mirrors and precision electroweak data, Phys. Rev. D **65**, 053002 (2002).
[129] J. Gu and L.-T. Wang, Sum rules in the standard model effective field theory from helicity amplitudes, J. High Energy Phys. 03 (2021) 149.
[130] M. E. Peskin and T. Takeuchi, Estimation of oblique electroweak corrections, Phys. Rev. D **46**, 381 (1992).
[131] B. Batell, S. Gori, and L.-T. Wang, Higgs couplings and precision electroweak data, J. High Energy Phys. 01 (2013) 139.
[132] S. Gori, J. Gu, and L.-T. Wang, The $Zb\bar{b}$ couplings at future e^+e^- colliders, J. High Energy Phys. 04 (2016) 062.
[133] A. Efrati, A. Falkowski, and Y. Soreq, Electroweak constraints on flavorful effective theories, J. High Energy Phys. 07 (2015) 018.
[134] A. Falkowski and F. Riva, Model-independent precision constraints on dimension-6 operators, J. High Energy Phys. 02 (2015) 039.
[135] S. Schael *et al.* (ALEPH, DELPHI, L3, OPAL, LEP Electroweak Collaboration), Electroweak measurements in electron-positron collisions at W-boson-pair energies at LEP, Phys. Rep. **532**, 119 (2013).
[136] A. M. Sirunyan *et al.* (CMS Collaboration), Search for single production of vector-like quarks decaying into a b quark and a W boson in proton-proton collisions at $\sqrt{s} = 13$ TeV, Phys. Lett. B **772**, 634 (2017).
[137] M. Buchkremer, G. Cacciapaglia, A. Deandrea, and L. Panizzi, Model-independent framework for searches of top partners, Nucl. Phys. **B876**, 376 (2013).
[138] J. Alwall, R. Frederix, S. Frixione, V. Hirschi, F. Maltoni, O. Mattelaer, H. S. Shao, T. Stelzer, P. Torrielli, and M. Zaro, The automated computation of tree-level and next-to-leading order differential cross sections, and their matching to parton shower simulations, J. High Energy Phys. 07 (2014) 079.
[139] ATLAS Collaboration, A detailed map of Higgs boson interactions by the ATLAS experiment ten years after the discovery, Nature (London) **607**, 52 (2022).
[140] CMS Collaboration, A portrait of the Higgs boson by the CMS experiment ten years after the discovery, Nature (London) **607**, 60 (2022).
[141] J. de Blas, Y. Du, C. Grojean, J. Gu, V. Miralles, M. E. Peskin, J. Tian, M. Vos, and E. Vryonidou, Global SMEFT fits at future colliders, in *2022 Snowmass Summer Study* (2022), 6, arXiv:2206.08326.
[142] M. Aaboud *et al.* (ATLAS Collaboration), Measurement of the W-boson mass in pp collisions at $\sqrt{s} = 7$ TeV with the ATLAS detector, Eur. Phys. J. C **78**, 110 (2018); **78**, 898 (E) (2018).
[143] R. Aaij *et al.* (LHCb Collaboration), Measurement of the W boson mass, J. High Energy Phys. 01 (2022) 036.
[144] C. W. Murphy, Bottom-quark forward-backward and charge asymmetries at hadron colliders, Phys. Rev. D **92**, 054003 (2015).
[145] B. Yan and C. P. Yuan, Anomalous $Zb\bar{b}$ Couplings: From LEP to LHC, Phys. Rev. Lett. **127**, 051801 (2021).
[146] H. Dong, P. Sun, B. Yan, and C. P. Yuan, Probing the $Zb\bar{b}$ anomalous couplings via exclusive Z boson decay, Phys. Lett. B **829**, 137076 (2022).
[147] B. Yan, Z. Yu, and C. P. Yuan, The anomalous $Zb\bar{b}$ couplings at the HERA and EIC, Phys. Lett. B **822**, 136697 (2021).
[148] H. T. Li, B. Yan, and C. P. Yuan, Jet charge: A new tool to probe the anomalous $Zb\bar{b}$ couplings at the EIC, Phys. Lett. B **833**, 137300 (2022).
[149] H. Cheng *et al.* (CEPC Physics Study Group Collaboration), The Physics potential of the CEPC. Prepared for the US Snowmass Community Planning Exercise (Snowmass 2021), in 2022 Snowmass Summer Study (2022), 5, arXiv:2205.08553.
[150] G. Bernardi *et al.*, The Future Circular Collider: A Summary for the US 2021 Snowmass Process, arXiv:2203.06520.